HYDRAULIC PERFORMANCE OF COANDA-EFFECT SCREENS

By Tony L. Wahl,[1] P.E., Member, ASCE

ABSTRACT: A theoretically based computational model is presented for predicting the hydraulic performance of Coanda-effect screens. These screens use a tilted-wire, wedge-wire screen panel to remove thin layers of high-velocity flow from the bottom edge of a supercritical flow. Typical slot openings are 1 mm or less, and the screens are self-cleaning with no moving parts. The discharge characteristics of several screen materials were evaluated in laboratory tests, and a relation was developed for computing the discharge through a tilted-wire screening surface as a function of the Froude number, the specific energy, and the Reynolds and Weber numbers. A model for the performance of complete Coanda-effect screen structures predicts the wetted length of screen required to accept a given flow, or the flow rate through the screen and the bypass flow over a screen that does not accept all of the flow. Predictions from the model compare favorably to results from clean-water laboratory tests of several different prototype-size screen structures. The model will allow designers to accurately size screens and evaluate design alternatives.

INTRODUCTION

There is a growing need on water resources projects to screen fine debris and small aquatic organisms from delivered flows. Unfortunately, with traditional screen designs, as the target of the screening effort becomes smaller, maintenance effort needed to keep screens clean is often dramatically increased and screen structures must be enlarged to keep through-screen velocities low. One screen design that offers potential for economically screening fine materials with a minimum of cleaning maintenance is the Coanda-effect screen, also known as the static inclined screen or sieve bend. Sieve bends have been used in the mining industry since about 1955 (Fontein 1965). Recently, this self-cleaning screen with no moving parts has been successfully used for debris and fish exclusion on several water resources projects [e.g., Strong and Ott (1988)], but there has been little detailed technical information available to hydraulic designers. Coanda-effect screens are commercially available, and manufacturers have cited screening capacities of 0.09–0.14 $m^3/s/m$ (1.0–1.5 $ft^3/s/ft$) of crest length, but much higher capacities have been observed in some prototype installations. Some aspects of the commercially available designs have been patented [H. E. Finch and J. J. Strong, ''Self-cleaning screen,'' U.S. Patent No. 4,415,462 (1983)].

The primary features of a Coanda-effect screen are illustrated in Fig. 1. The screen is installed on the downstream face of an overflow weir. Flow passes over an acceleration plate, and then across the wedge-wire screen panel. Wires are horizontal, perpendicular to the flow across the screen. The acceleration plate can be an ogee-shaped profile or a simple circular arc; the objective is to provide a smooth acceleration of the flow and deliver it tangent to the screen surface at the upstream edge. Typically, the screen panel is a concave arc with a radius of curvature of approximately 3 m, although planar screen panels can also be used. Flow passing through the screen (screened flow) is collected in a conveyance channel beneath the screen, while overflow, fish, and debris pass off the downstream end of the screen. Flow velocities across the screen are typically 2–3 m/s (6.5–10 ft/s), increasing toward the toe of the screen. Froude numbers across the screen surface can vary from about 2 to 30 or greater, with the largest Froude numbers obtained when there is minimal bypass flow, or overflow, off the toe of the screen, and thus shallow flow depths and high velocities at the screen toe. Commercially available designs typically have the screen inclined at 60° from horizontal at the upstream edge, and have a total head drop across the structure of about 1.2–1.5 m (4–5 ft).

Coanda-effect screens utilize a unique tilted-wire screen panel. The individual wires are tilted a few degrees downstream (Fig. 1) to produce shearing offsets into the flow above the screen. The typical tilt angle is 5°, but angles of 3° to 6° are available from most screen manufacturers. Slot widths are typically 1 mm (0.04 in.) or less. The shearing action is enhanced by the fact that flow remains attached to the top surface of each wire, and is thus directed into the offset created at the next downstream wire. This attachment of the flow to the top surface of each wire is an example of the Coanda effect, the tendency of a fluid jet to remain attached to a solid flow boundary. A detailed discussion of the Coanda effect and its application to tilted-wire screens is provided by Wahl (1995).

MODELING FLOW OVER COANDA-EFFECT SCREEN STRUCTURE

A significant obstacle to application of Coanda-effect screens has been the inability to accurately predict the flow capacity of specific screen designs. The objective of the model presented here is to predict the discharge through the screen and the overflow off the screen; these are the variables of primary interest in most water resources applications. Because

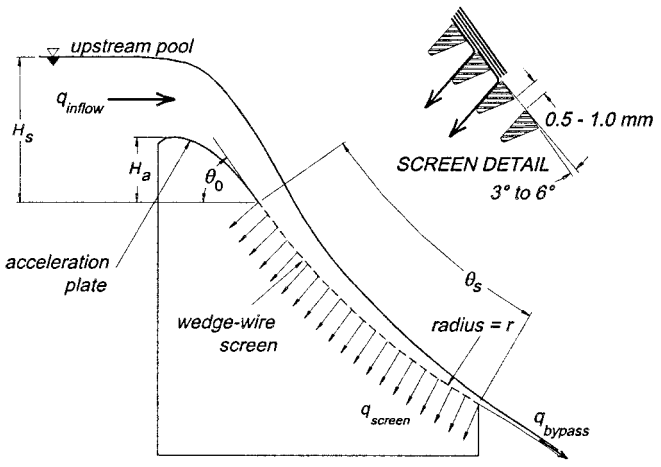

FIG. 1. Features, Typical Arrangement, and Design Parameters for Coanda-Effect Screens

[1]Hydr. Engr., U.S. Bureau of Reclamation, Water Resour. Res. Lab., Mail Code D-8560, P.O. Box 25007, Denver, CO 80225-0007. E-mail: twahl@do.usbr.gov

Note. Discussion open until November 1, 2001. To extend the closing date one month, a written request must be filed with the ASCE Manager of Journals. The manuscript for this paper was submitted for review and possible publication on August 22, 2000; revised January 18, 2001. This paper is part of the ***Journal of Hydraulic Engineering***, Vol. 127, No. 6, June, 2001. ©ASCE, ISSN 0733-9429/01/0006-0480–0488/$8.00 + $.50 per page. Paper No. 22449.

these screens are substantially self-cleaning, the first effort has been to develop a model applicable to clean screens.

Fig. 2 shows details of the screen material. The wire tilt angle is designated by ϕ, while w and s are the wire and slot widths, respectively. The effective height of the offset created at the leading edge of each wire is

$$y_{off} = (s + w \cos \phi)\sin \phi \tag{1}$$

or, if the tilt angle is relatively small ($\phi \leq 7°$), y_{off} can be approximated within 1% as $(w + s)\phi$, with ϕ expressed in radians. Coanda-effect screens should be constructed using a wire whose upstream edges are sharp; a rounded edge will reduce the effectiveness of the shearing offset.

Flow over a Coanda-effect screen structure is spatially varied with decreasing discharge, and can be modeled using the energy equation, accounting for the changing discharge along the length of the screen (Chow 1959). Referring to the control volume in Fig. 2, the energy equation is

$$(s + w)\theta + D_1 \cos \theta + \alpha \frac{V_1^2}{2g} = D_2 \cos \theta + \alpha \frac{V_2^2}{2g} + S_f(s + w) \tag{2}$$

where θ = inclination angle of the screen panel; α = energy coefficient (hereafter assumed to be 1.0); D_1 and D_2 = flow depths normal to the screen face; V_1 and V_2 = flow velocities; g = acceleration of gravity; and S_f = friction slope. Eq. (2) can be rearranged to obtain

$$D_2 = (s + w)\tan \theta + D_1 + \alpha \frac{(q_1^2/D_1^2 - q_2^2/D_2^2)}{2g \cos \theta} - S_f \frac{s + w}{\cos \theta} \tag{3}$$

where q_1 and q_2 = unit discharges at the upstream edges of two adjacent wires. The discharge at the downstream wire is $q_2 = q_1 - \Delta q$, where Δq is the discharge through the slot. Choosing an appropriate friction model for computation of S_f and assuming that Δq can be determined separately, (3) can be solved numerically for D_2.

DISCHARGE THROUGH TILTED-WIRE SCREENS

To implement the model described above, a relation for Δq is needed. The discharge through isolated floor slots in subcritical and supercritical flows has been studied by several investigators [e.g., Venkataraman (1977), Nasser et al. (1980), and Ramamurthy et al. (1994)]. These investigators related the discharge coefficient of the slot to the Froude number or quantities related to the Froude number. None of these studies considered the effects of an offset into the flow. Flows over and through screens installed in the floor of a conveyance channel have been studied by Noseda (1955), Miao (1958), and Babb and Schlenker (1999). Miao noted that friction could be neglected when modeling the flow profile over a mesh screen, since the flow removed by the screen prevents development of a normal boundary layer and flow profile. Babb and Schlenker studied supercritical flows over perforated plate screens used in fish separation facilities and found that the discharge coefficient could be approximated by a power curve function of the Froude number F for flows between F = 1.2 and F = 10.

Fontein (1965) identified gravitational, viscous, and surface tension forces, as well as air entrainment and wire shape as significant factors affecting the discharge through sieve bends used for dewatering mining slurries. Fontein evaluated the effects of the Froude and Reynolds numbers quantitatively, and the effect of the Weber number was evaluated qualitatively in tests of clean and greased-surface screens. Debris exclusion performance was affected by viscous forces and was thus a function of the Reynolds number R. To maintain self-cleaning, Fontein recommended R > 1,000, with R = Vs/ν, where V is the velocity across the screen, s is the slot width, and ν is the kinematic viscosity.

For the present study, the discharge through each slot of a tilted-wire screen was modeled by considering Fig. 3, showing a velocity vector approaching a single slot opening. The resultant vector $\mathbf{V}_r$ is made up of the component tangent to the screen surface V and the potential velocity normal to the screen surface due to hydrostatic pressure and streamline curvature $[2g(D \cos \theta + V^2D/(gr))]^{1/2}$, where r is the radius of curvature of the screen. For planar screens, $D \cos \theta$ is the hydrostatic pressure head at the screen face, and for curved screens, $V^2D/(gr)$ is the change in pressure head caused by streamline curvature (positive for concave screens, negative for convex screens). Recognizing that the specific energy is $E = \alpha V^2/(2g) + D \cos \theta + V^2D/(gr)$, with $\alpha = 1.0$ for accelerating flows, the magnitude of $\mathbf{V}_r$ is

$$\mathbf{V}_r = \sqrt{V^2 + 2g(D \cos \theta + V^2D/(gr))} = \sqrt{2gE} \tag{4}$$

The deviation of $\mathbf{V}_r$ from the tangential direction (i.e., from a line through the leading edge of each wire) is the angle δ in Fig. 3, and can be computed from

$$\delta = \tan^{-1}(\sqrt{2g(D \cos \theta + V^2D/gr)}/V) \tag{5}$$

which can also be expressed in terms of the Froude number modified to include the effects of streamline curvature F = $V/[g(D \cos \theta + V^2D/(gr))]^{1/2}$, as

$$\delta = \tan^{-1}(\sqrt{2}/\mathrm{F}) \tag{6}$$

The opening between two wires is shown in Fig. 4. The opening consists of both the width of the slot and the height

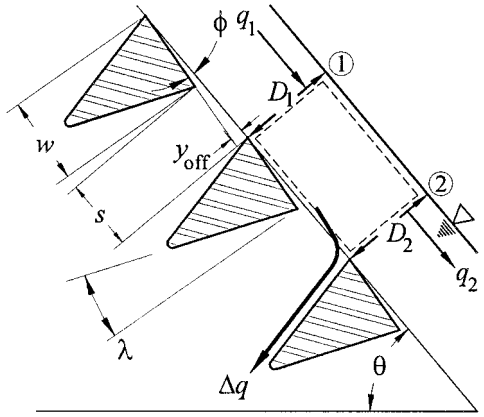

FIG. 2. Screen Geometry and Control Volume for Analysis of Flow through Tilted-Wire Screen

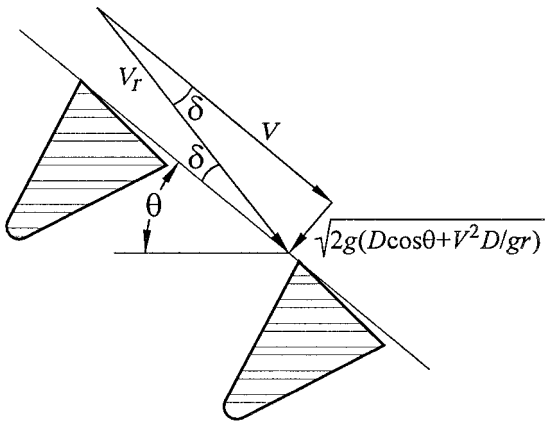

FIG. 3. Velocity Vector Approaching Tilted-Wire Screen

of the offset created by the tilting of the wires. The length of line AB is the effective length of the slot $s' = (s^2 + y_{off}^2)^{1/2}$. The deviation of line AB from a line tangent to the screen face is the angle ψ, and the deviation from a line parallel to the top edge of a given wire is ε. The value of ψ can be determined by noting that $\varepsilon = \psi + \phi$ and $\varepsilon = \tan^{-1}(y_{off}/s)$.

Fig. 5 shows the velocity vector $\mathbf{V}_r$ and the slot opening. The angle between the two is $\delta + \psi$, and the flow rate through the opening can be computed from

$$\Delta q = C_{cv} s' \mathbf{V}_r \sin(\delta + \psi) \tag{7}$$

where C_{cv} = coefficient that accounts for the effects of velocity reduction and contraction of the flow through the slot. Recalling that $\psi = \varepsilon - \phi$, making use of trigonometric identities, and substituting (6) for δ, one can show that

$$\sin(\delta + \psi) = \sqrt{\frac{2}{2 + \mathsf{F}^2}} \cos(\varepsilon - \phi) + \sqrt{\frac{\mathsf{F}^2}{2 + \mathsf{F}^2}} \sin(\varepsilon - \phi) \tag{8}$$

For a given screen material, $\varepsilon - \phi$ is constant, so $\sin(\delta + \psi)$ is solely a function of the Froude number. If one denotes this expression as C_{F} one can rewrite (7) as

$$\Delta q = C_{cv} C_{\mathsf{F}} s' \sqrt{2gE} \tag{9}$$

which has the familiar form of the equation for discharge through an orifice, when one considers the quantity $C_{cv}C_{\mathsf{F}}$ to be equivalent to a discharge coefficient C_d. In the traditional orifice equation the discharge coefficient is composed of the product of a separate velocity coefficient and contraction coefficient, and one could argue that there should be separate coefficients in (9). However, it was not possible in the current study to isolate the contraction and velocity-reduction effects, so both effects are represented in the C_{cv} coefficient.

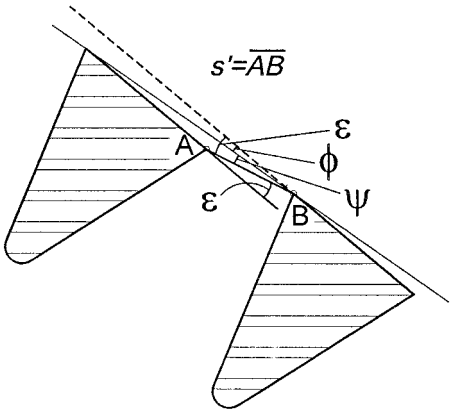

FIG. 4. Screen Slot Geometry

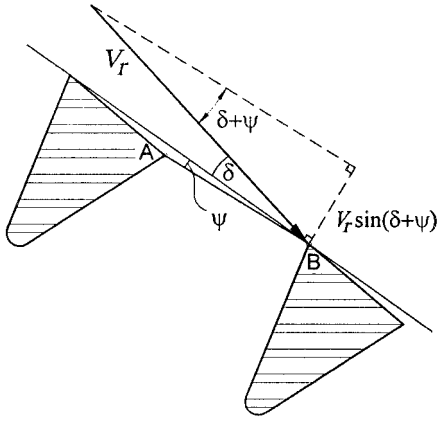

FIG. 5. Approach Velocity Vector and Screen Slot

Variation of C_{F}

The physical meaning of the $2/(2 + \mathsf{F}^2)$ and $\mathsf{F}^2/(2 + \mathsf{F}^2)$ terms in (8) can be better understood by substituting the Froude number $\mathsf{F} = V/(gD \cos\theta)^{1/2}$ into the specific energy equation (neglecting the terms associated with streamline curvature for simplicity)

$$E = D\cos\theta + \frac{V^2}{2g} = D\cos\theta + \frac{\mathsf{F}^2 gD\cos\theta}{2g}$$

$$= D\cos\theta \left(1 + \frac{\mathsf{F}^2}{2}\right) \tag{10a}$$

$$D\cos\theta = E\left(\frac{2}{2 + \mathsf{F}^2}\right) \tag{10b}$$

This shows that $2/(2 + \mathsf{F}^2)$ is the depth-energy fraction, the fraction of the total specific energy associated with the flow depth (and the change in pressure due to streamline curvature, if that were also included). Similarly, $\mathsf{F}^2/(2 + \mathsf{F}^2)$ is the kinetic-energy fraction, the fraction of the total specific energy associated with the velocity head. The relative size of the depth-energy fraction and kinetic-energy fraction and the characteristics of the screen surface determine whether the opening behaves primarily as an orifice (discharge proportional to $D^{1/2}$) or a series of shearing offsets (discharge proportional to V).

The value of C_{F} indicates the screening capacity of a slot opening as a function of the Froude number, while $C_{\mathsf{F}} \times p$ is an indicator of the performance of the entire screen surface, accounting for differences in screen porosity $p = s/(s + w)$. Fig. 6 shows the variation of C_{F} [Fig. 6(a)] and $C_{\mathsf{F}} \times p$ [Fig. 6(b)] as a function of the Froude number and compares the C_{F} and $C_{\mathsf{F}} \times p$ versus F relations for several hypothetical screens, demonstrating the effects of changing the wire tilt angle, slot width, and wire width. Values of C_{F} are nearly independent of changes in screen geometry at low Froude numbers, where orifice flow dominates. At high Froude numbers, C_{F} increases with increasing wire tilt, decreasing slot width, and increasing wire width. At high Froude numbers, the value of $C_{\mathsf{F}} \times p$ is directly proportional to the wire tilt angle, and nearly independent of the wire width and slot width, since changes in the value of C_{F} as a function of these parameters are offset by the changing porosity. At low Froude numbers, orifice-type flow dominates and $C_{\mathsf{F}} \times p$ is insensitive to the tilt angle, but directly proportional to the porosity.

It should also be noted that for $\mathsf{F} > 1$, the curves shown in Fig. 6 could be approximated by a power curve function, similar to the formulation proposed by Babb and Schlenker (1999) for discharge coefficients of perforated plate screens supporting supercritical flows. This suggests that similar flow mechanics may govern the screening of supercritical flows through tilted-wire screens and perforated plate screens. The

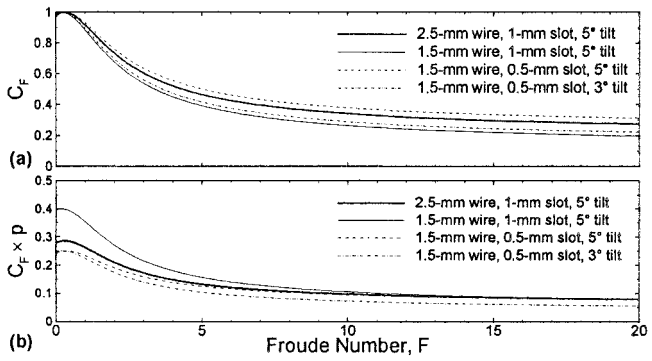

FIG. 6. Variation of C_{F} and $C_{\mathsf{F}} \times p$ versus Froude Number

formulation proposed here has the advantage that for $F < 1$, C_F reaches a maximum value and then decreases slightly approaching $F = 0$, while a power curve relation would predict an infinite discharge coefficient at $F = 0$.

Values of C_{cv}

To determine values of C_{cv}, a test facility (Fig. 7) was constructed in which the flow through small samples of three different screens could be measured over a range of Froude numbers from about 2.5 to 16. The testing was performed in the Bureau of Reclamation's Water Resources Research Laboratory in Denver. The tested screens were 7.5–10 cm square or rectangular samples provided by screen manufacturers. Relevant screen dimensions are summarized in Table 1.

Dimensions and related uncertainties for the wire widths and slot widths of each screen were determined by measurement at 20 to 30 locations on each screen with a micrometer. Wire tilt angles were measured using two different techniques: (1) an optical comparator (screens 2 and 3); and (2) an optical reflection technique in which light from a laser pointer was reflected off the screen face so that the measured deflection of the beam could be used to compute the tilt of the wire (all screens). The measurements with the optical comparator were made by the National Institute of Standards and Technology, Gaithersburg, Md., and have an estimated expanded uncertainty of ±0.1° (95% confidence level). Measurements by the laser method were made at the Bureau of Reclamation and have an estimated uncertainty of ±0.25°. The optical comparator can only measure the tilt angle at the cut edges of the screen, while the laser method can be used at essentially any location on the screen. The reference line (zero tilt) for the measurements with the optical comparator was a line through the two high points of a screen over its full length (screens were slightly warped in some cases). For the laser method, the zero-reference was defined by laying a small mirror across the top of several wires at the location where the tilt was being measured and marking the location of the beam reflected by the mirror.

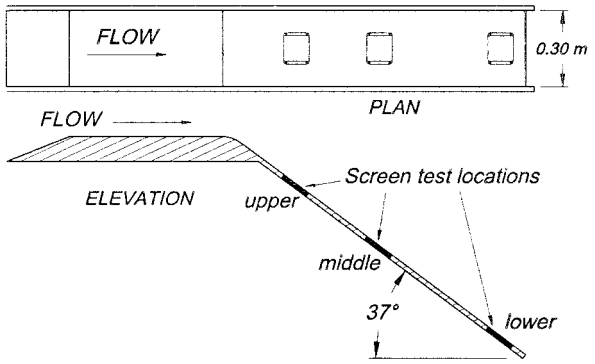

FIG. 7. Schematic Diagram of Screen-Test Facility Used to Determine C_{cv} Values

Columns 4, 6, and 8 in Table 1 provide the variabilities of the wire width, slot width, and tilt angle, and the uncertainties of the mean values used in subsequent calculations. The variability is the estimated point-to-point variation of the parameter over the screen surface, expressed at a 95% confidence level after factoring out the uncertainty associated with the measurement methods. Variability of the tilt angle for all screens was significantly greater than the uncertainty of either of the two methods used to measure wire tilt. The tilt angles determined using the laser-pointer method are shown in Table 1 and were used in all subsequent work described in this paper, primarily because this method could be applied to the entire screen surface, rather than just the cut edges of the screen. For comparison, the average tilt angles measured with the optical comparator on the edges of screens 2 and 3 were 3.38° and 5.71°, with wire-to-wire variabilities of 1.28° and 1.22°, respectively. For screen 2 the agreement between the two methods is excellent, while for screen 3 the difference in mean tilt angles is believed to be the result of measuring only at the cut edge of the screen with the optical comparator.

The test facility for determining values of C_{cv} consisted of a flume, 20 m long by 0.91 m wide, leading the flow to a 0.30 m-wide test section. Flow entered the test section over a short section of ogee-shaped crest leading to a sloped ramp inclined 37° from horizontal (Fig. 7). Screens were installed flush with the floor of the sloped flume at three locations. The upper location was approximately 20 cm (vertical) below the horizontal crest, and the lower location was about 81 cm below the horizontal crest. The third test location was added late in the test program about 45 cm below the horizontal crest. Crest lifts were also installed in increments of 1.9 cm each during later tests to produce flows with intermediate drop heights. Flows ranging from 0.023 to 0.46 $m^3/s/m$ could be delivered to the test section. Flow rates into the test facility were measured with the laboratory's fixed Venturi meters, which have a measurement uncertainty of $<\pm 0.5\%$.

Below the screen test location, a flow divider plate and collector box captured the flow passing through the screen and directed it to measurement locations. The position of the divider plate was varied slightly for each screen, but was generally about 2 to 3 cm from the leading edge of the screen. The divider plate allowed the flow through the first few screen slots to be measured separately from the flow through the downstream portion of the screen, with only the flow through the downstream portion of the screen used to compute values

TABLE 1. Screen Dimensions for Tests to Determine C_{cv}

Screen number	Screen description	WIRE WIDTH w (mm) Mean	WIRE WIDTH w (mm) Variability Uncertainty of mean	SLOT WIDTH s (mm) Mean	SLOT WIDTH s (mm) Variability Uncertainty of mean	TILT ANGLE ϕ Mean (deg)	TILT ANGLE ϕ Variability Uncertainty of mean (deg)	Screen porosity $s/(s + w)$	Support rod spacing (mm)
1	2.38 mm (3/32 in.) wire, 1 mm slots, 7.7 cm × 9.2 cm	2.390	±0.015 ±0.003	1.021	±0.094 ±0.019	3.82	±0.63 ±0.08	0.299	70
2	1.52 mm (0.060 in.) wire, 1 mm slots, 10.4 cm × 7.2 cm	1.549	±0.010 ±0.001	0.993	±0.035 ±0.006	3.37	±1.39 ±0.14	0.390	19
3	1.52 mm (0.060 in.) wire, 0.5 mm slots, 7.4 cm × 8.7 cm	1.496	±0.015 ±0.003	0.467	±0.034 ±0.006	6.88	±0.99 ±0.13	0.238	14

of C_{cv}. Thus, the test section was representative of a section of a continuous screen panel. The flow through the first few screen slots was significantly lower than that through the downstream slots.

Flow through the section of the screen upstream from the divider plate was measured using a stopwatch and a 4-L graduated cylinder. Flow rates through the test portion of the screen, downstream from the divider plate, were measured using a half-90° V-notch weir.

The flow velocity above the screen face was measured at the downstream edge of the screen, using a 4.7 mm diameter pitot tube with a stagnation port diameter of 0.75 mm. Measurements were made about 6 mm above the screen face, except when shallow flow depths required lowering the pitot tube to keep it in the flow. It is recognized that the pitot tube is a less than ideal instrument for measuring velocity in supercritical flows due to the potential for flow separation from the leading edge of the tube and from the vertical stem. However, the pitot tube worked well for these tests and was much more practical (economically and operationally) than other alternatives, such as a noninvasive laser Doppler velocimeter. Flow profiles versus depth confirmed that this was an appropriate measurement technique, indicating that the velocity was essentially uniform immediately downstream from the screen, as one would expect due to the accelerating flow and continual removal of the boundary layer by the screen.

The velocity at the upstream edge of the screen was computed by applying the energy equation between the upstream and downstream edges of the screen. Velocity measurements made at the upstream and downstream edges of the screen during shakedown testing confirmed that this yields an accurate estimate of the upstream velocity. The velocity data and the measured discharges were used to compute flow depths and Froude numbers at the upstream and downstream ends of the test section, and average values were computed from the upstream and downstream values. The average values are plotted in the figures presented below.

During shakedown testing, screens were tested with various widths open to the flow and the excess width masked off by tape. These tests showed that the underlying support rods had no effect on the flow, i.e., the point of flow control was at or near the face of the screen. The position of the flow divider was also varied during shakedown testing to ensure that the test section was representative of a portion of a continuous screen.

Fig. 8 shows the values of $C_F C_{cv}$ for the three tested screens as a function of the Froude number. Screens 2 and 3 were tested only at the upper ($F = 2.5–10$) and lower ($F = 7–16$) positions, while screen 1 was tested at all three positions and with variable crest heights. Velocities across the screens ranged from about 2.1 to 4.4 m/s (6.8 to 14.4 ft/s). Error bars indicate 95% uncertainty estimates propagated from uncertainties in the underlying measurements of discharge and velocity.

The form of the $C_F C_{cv}$ versus F curves is similar to Fig. 6, which showed C_F versus F, but there are obviously significant differences in C_{cv} at the different test locations, as indicated by the distinct groupings of $C_F C_{cv}$ values. For screens 2 and 3 there are two separate curves that do not coincide in the range of overlapping Froude numbers (about $F = 7$ to $F = 10$) that could be obtained at the upper and lower test positions. There are also separate curves for screen 1, although the differences are less distinct because tests were conducted at all three positions and with variable drop heights. Recalling that C_F is solely a function of the Froude number for any specific screen, the differences in the values of $C_F C_{cv}$ at a given Froude number must be due to differences in the C_{cv} values at the different velocities produced by changing the drop height to the screen. These differences can be related to dimensionless parameters of the flow.

The computed values of C_{cv} were found to vary as a function of several dimensionless parameters, including the Reynolds number R, the Weber number W, the Froude number F, and the ratio R/W, which indicates the relative influence of viscous and surface tension forces and for a given fluid is a function solely of the velocity. The Reynolds number was computed using the tangential velocity (i.e., the velocity measured by the pitot tube), and the slot width of the screen, $R = Vs/\nu$. The Weber number is $\rho V^2 s/\sigma$, where ρ is the fluid density and σ is the surface tension constant ($\sim$0.073 N/m). Several regression relations involving these parameters were explored, and the best relation for predicting C_{cv} was

$$C_{cv} = 0.210 + 0.0109(R/W) + 0.00803(F) \qquad (11)$$

The prediction performance of this relation is shown in Fig. 9. Horizontal error bars indicate uncertainty estimates for the measured C_{cv} values. Vertical error bars indicate uncertainty in the predicted C_{cv} values caused by underlying uncertainty in the values of F, R, and W.

IMPLEMENTING NUMERICAL MODEL

The model for screen structure performance summarized in Eqs. (3), (7), (8), (9), and (11) was implemented in a computer program. The model predicts the flow rate through the screen and the overflow off the toe of the screen, and provides detailed information on the flow depths and velocities along the length of the screen. The model uses unit discharge quantities.

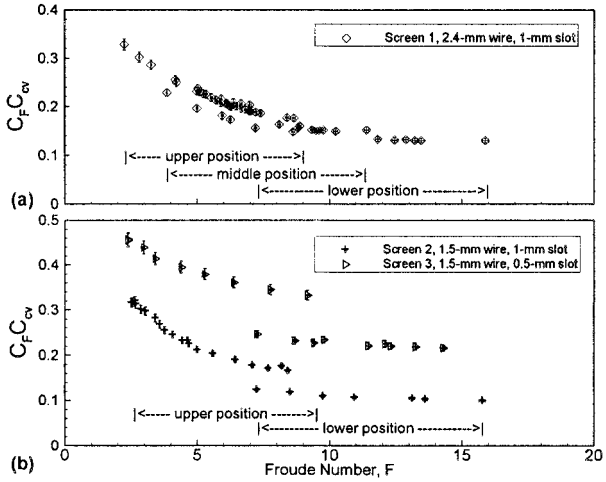

FIG. 8. Variation of $C_F C_{cv}$ versus Froude Number for: (a) Screen 1; (b) Screens 2 and 3

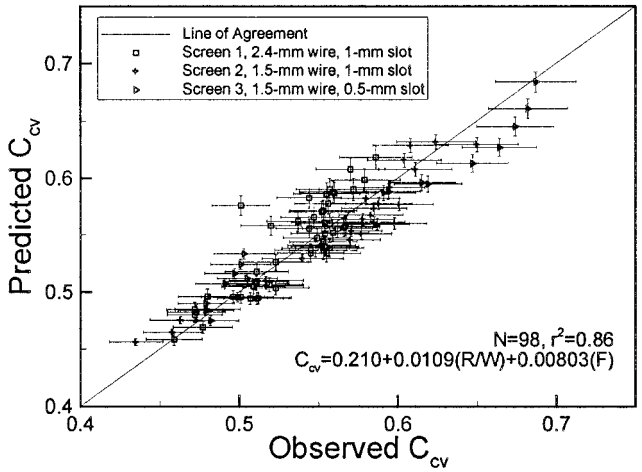

FIG. 9. Comparison of Observed Values of C_{cv} with Those Predicted Using Regression Eq. (11)

Computation of the flow profile begins with the assumption of potential flow over the crest and acceleration plate. The energy equation is used to determine the flow depth and velocity at the downstream edge of the acceleration plate, where the velocity profile is assumed to be uniform with depth, due to the inherent thinning of the boundary layer in an accelerating flow. Measurements of velocity profiles with the pitot tube verified this assumption.

Computations proceed wire-by-wire down the face of the screen, with the model determining the increment of flow diverted through the screen surface at each slot and the depth and velocity of the flow remaining above the screen. Calculations continue until all flow passes through the screen, or until the end of the screen is reached.

Effects of Friction on Flow Profile

The continuous removal of the bottom layer of the flow through the screen suggests that the development of a typical open-channel flow profile will not occur, and the effect of friction on the flow profile might be reduced or absent. To test this hypothesis, velocity profiles were measured with the pitot tube described earlier on one specific screen structure (configuration A-45 in Table 2) operating at a unit inflow of 0.117 $m^3/s/m$ (1.26 $ft^3/s/ft$). The measured profile is compared in Fig. 10 to velocity profiles computed with and without friction, using the Manning equation to compute S_f. An arbitrary roughness coefficient of $n = 0.012$ was selected for the profile computed with friction. With friction included, the velocity goes to zero at the end of the wetted section. The measured velocity profile and the profile computed without frictional effects do not exhibit this characteristic, and are substantially in agreement. Thus, friction can be neglected when computing the flow profile with (3).

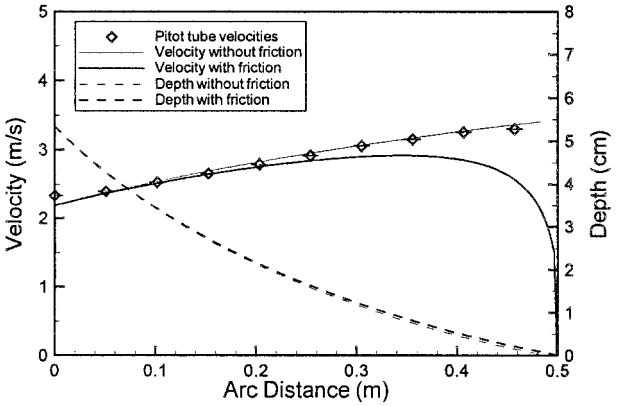

FIG. 10. Comparison of Measured and Computed Velocity Profiles

COMPARING NUMERICAL MODEL TO EXPERIMENTAL DATA

Several Coanda-effect screen structures have been tested in recent years by the Bureau of Reclamation (Wahl 1995, 2000), and the data collected offer a means for testing the performance of the numerical model developed here. Details of the tested screen structure dimensions and screen material properties are given in Tables 2 and 3, respectively. Table 4 shows the results of each test. Most screens were tested over a range of discharges up to a 50% bypass flow condition. All tests were conducted with clean screens and clear water, and in these prototype-size structures there was no air entrainment in the flow over the screens. For structures with greater drop heights than those tested, air entrainment might occur near the toe of the screen, and this would significantly affect screen performance.

Fig. 11 compares the screen performance predicted by the model to the observed performance for 97 of the 103 tests listed in Table 4 (63 cases without bypass flow, 40 cases with bypass flow). In the remaining 6 cases, the numerical model predicted slight overflow where none occurred, or did not predict overflow where slight overflow did occur, thus preventing direct comparison of the results. The agreement between the model and the experimental data is good throughout the range

TABLE 2. Coanda-Effect Screen Structure Dimensions

Screen	Initial incline θ_0 (deg)	Arc radius r (m)	Test width (m)	Acceleration plate configuration	Drop height (crest to top of screen) H_a (m)	Structure designation (Table 4)	θ_s (deg)	Arc length (m)
A (1 mm)	60	2.54	0.30	Ogee crest (design head 0.14 m)	0.37	A-60-1	25.0	1.12
						A-60-2	13.8	0.61
						A-60-3	10.3	0.46
A (1 mm)	55	2.54	1.42	Ogee crest (design head 0.19 m)	0.24	A-55	10.3	0.46
A (1 mm)	50	2.54	0.30	Ogee crest (design head 0.29 m)	0.25	A-50-1	25.0	1.12
						A-50-2	10.3	0.46
A (1 mm)	45	2.54	0.61	Ogee crest (design head 0.23 m)	0.13	A-45	13.8	0.61
B (0.5 mm)	60	3.05	0.61	Circular arc (0.30 m radius)	0.24	B-60	11.5	0.61

TABLE 3. Coanda-Effect Screen Material Properties

		WIRE WIDTH w (mm)		SLOT WIDTH s (mm)		TILT ANGLE ϕ			
			Variability		Variability		Variability		
Screen	Nominal dimensions	Mean	Uncertainty of mean	Mean	Uncertainty of mean	Mean (deg)	Uncertainty of mean (deg)	Screen porosity $s/(s + w)$	Support rod spacing (mm)
A	1.52 mm (0.060 in.) wire, 1 mm slots	1.516	±0.026 ±0.005	0.979	±0.060 ±0.011	6.81	±1.15 ±0.14	0.391	19
B	1.52 mm (0.060 in.) wire, 0.5 mm slots	1.584	±0.026 ±0.005	0.535	±0.112 ±0.020	4.90	±1.25 ±0.24	0.252	37

TABLE 4. Data Collected From Laboratory Tests of Coanda-Effect Screen Structures

Structure (Table 2)	q_{inflow} ($m^3/s/m$)	Wetted flow distance (m)	q_{screen} ($m^3/s/m$)
A-60-1	0.035	0.17	—
A-60-1	0.040	0.18	—
A-60-1	0.044	0.19	—
A-60-1	0.048	0.22	—
A-60-1	0.052	0.24	—
A-60-1	0.056	0.25	—
A-60-1	0.064	0.25	—
A-60-1	0.071	0.31	—
A-60-1	0.077	0.31	—
A-60-1	0.085	0.34	—
A-60-1	0.095	0.37	—
A-60-1	0.102	0.41	—
A-60-1	0.108	0.41	—
A-60-1	0.112	0.42	—
A-60-1	0.117	0.43	—
A-60-1	0.120	0.44	—
A-60-1	0.121	0.44	—
A-60-1	0.150	0.51	—
A-60-1	0.171	0.56	—
A-60-1	0.191	0.61	—
A-60-1	0.220	0.69	—
A-60-1	0.224	0.66	—
A-60-1	0.260	0.79	—
A-60-2	0.178	—	0.176
A-60-2	0.180	—	0.174
A-60-2	0.185	—	0.178
A-60-2	0.190	—	0.181
A-60-2	0.204	—	0.185
A-60-2	0.215	—	0.190
A-60-2	0.216	—	0.192
A-60-2	0.230	—	0.196
A-60-2	0.242	—	0.196
A-60-3	0.122	—	0.114
A-60-3	0.125	—	0.119
A-60-3	0.129	—	0.121
A-60-3	0.135	—	0.123
A-60-3	0.148	—	0.128
A-60-3	0.167	—	0.133
A-60-3	0.183	—	0.138
A-60-3	0.216	—	0.145
A-55	0.018	0.10	—
A-55	0.038	0.23	—
A-55	0.061	0.31	—
A-55	0.080	0.38	—
A-50-1	0.038	0.22	—
A-50-1	0.048	0.25	—
A-50-1	0.059	0.29	—
A-50-1	0.073	0.33	—
A-50-1	0.093	0.41	—
A-50-1	0.116	0.48	—
A-50-1	0.141	0.56	—
A-50-1	0.163	0.61	—
A-50-1	0.176	0.64	—
A-50-1	0.188	0.66	—
A-50-1	0.209	0.74	—
A-50-1	0.241	0.79	—
A-50-1	0.261	0.86	—
A-50-1	0.284	0.91	—
A-50-1	0.301	0.97	—
A-50-1	0.328	1.02	—
A-50-1	0.340	1.07	—
A-50-1	0.373	—	0.359
A-50-1	0.389	—	0.366
A-50-2	0.107	—	0.106
A-50-2	0.156	—	0.130
A-50-2	0.166	—	0.134
A-50-2	0.220	—	0.151
A-45	0.024	0.15	—
A-45	0.039	0.20	—
A-45	0.059	0.28	—
A-45	0.060	0.28	—
A-45	0.070	0.32	—
A-45	0.085	0.36	—
A-45	0.098	0.41	—
A-45	0.110	0.43	—
A-45	0.135	0.51	—
A-45	0.164	—	0.162
A-45	0.168	—	0.162
A-45	0.184	—	0.173
A-45	0.189	—	0.171
A-45	0.190	—	0.172
A-45	0.192	—	0.175
A-45	0.192	—	0.177
A-45	0.196	—	0.175
A-45	0.197	—	0.176
A-45	0.202	—	0.169
A-45	0.206	—	0.177
A-45	0.216	—	0.185
A-45	0.249	—	0.194
B-60	0.025	0.14	—
B-60	0.038	0.21	—
B-60	0.046	0.24	—
B-60	0.050	0.25	—
B-60	0.064	0.32	—
B-60	0.072	0.36	—
B-60	0.077	0.38	—
B-60	0.086	0.41	—
B-60	0.105	0.47	—
B-60	0.129	0.58	—
B-60	0.141	—	0.131
B-60	0.158	—	0.136
B-60	0.174	—	0.142
B-60	0.182	—	0.145

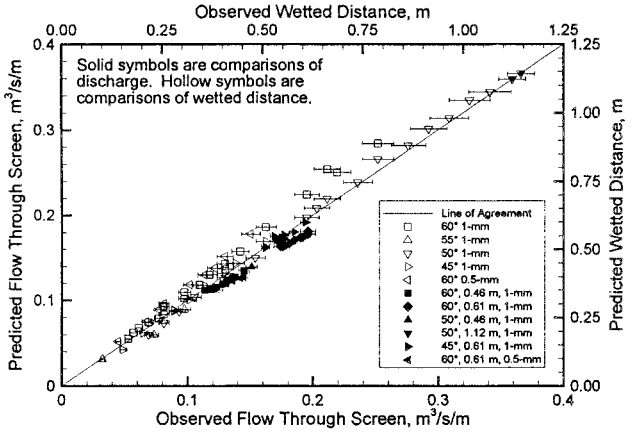

FIG. 11. Comparison of Laboratory Results and Predictions from Numerical Model

of flow conditions. It should be emphasized that this agreement was obtained without the need for further calibration of the model beyond the development of the regression relation for C_{cv} [(11)].

All of the test data shown in Fig. 11 were obtained from concave screens. The effects of screen curvature were accounted for in (4), and are significant. The predicted flow rates through the screens would be reduced by about 10% if the effects of screen curvature were neglected.

EXAMPLE APPLICATION

Capacities of screens with significant drop heights can be large. For example, the numerical model was applied to a hypothetical structure using a screen with a 1 mm slot width, 1.524 mm-wide wires, a 5° wire tilt angle, 3.05 m (10 ft) screen arc radius, and an initial screen inclination of $\theta_0 = 60°$. The drop height from the crest of the acceleration plate to the

top edge of the screen was assumed to be 0.24 m (0.8 ft). The screen was assumed to span an arc of $\theta_s = 25°$, producing a total arc length of 1.33 m (4.36 ft). Similar designs are commercially available.

The capacity of this example screen is predicted to be 0.368 $m^3/s/m$ (3.96 $ft^3/s/ft$) at a zero-bypass flow condition, and 0.394 $m^3/s/m$ (4.25 $ft^3/s/ft$) at a 10% bypass rate. Changing the slot width to 0.5 mm and holding all other parameters constant changes the zero-bypass capacity to 0.313 $m^3/s/m$ (3.37 $ft^3/s/ft$) and the 10% bypass capacity to 0.322 $m^3/s/m$ (3.47 $ft^3/s/ft$)—reductions of 15 and 18%, respectively. These are relatively small changes compared to the 38% reduction in screen porosity corresponding to this change in slot width. This result is consistent with the earlier discussion of the variation of $C_F \times p$ and its insensitivity to changes in slot width and wire size.

The potential for high-flow capacity is an important consideration for screen designers. Overflow may be needed to carry debris downstream to a waste channel or to maintain a wetted screen surface and ensure safe downstream passage of fish. If capacity is underestimated, modification of the structure may be required, e.g., blocking a portion of the screen length. Additionally, knowledge of high-screen capacity may permit the use of a structure with a shorter crest length or lower drop height, which may yield economic savings or make a structure feasible at a site with limited available head or restricted construction space.

EFFECT OF VARYING DESIGN PARAMETERS

The numerical model presented in this paper can be used to examine the options available to designers when developing customized designs. Key parameters that designers might wish to vary include screen slot width and wire size, wire tilt angle, screen arc radius, screen inclination, drop height from top of crest to start of screen, and total drop height across the screen structure.

Screen Slot Width and Wire Size

The example given earlier showed that changing slot widths or wire sizes (and thus porosity) does affect flow capacity, but to a lesser degree than might be expected. The effects are most significant at high bypass ratios, which produce the lowest Froude numbers over the screen. In general, designers should make an initial selection of wire size and slot width with primary consideration for durability, constructability, and debris exclusion characteristics. Designs can then be fine-tuned if necessary to increase or decrease flow capacity.

Wire Tilt Angle

The wire tilt angle directly affects screen capacity because the offset height is proportional to the tilt angle [(1)]. A tilt angle of 5° has been used in most Coanda-effect screen installations to date. There may be disadvantages to increasing the tilt angle, such as increased debris retention caused by a higher offset height and a reduced ability to exclude small debris. As an upper limit, the tilt angle should always be less than the relief angle of the wire λ (Fig. 2). Typical relief angles are 10° to 15°, although wires with relief angles as small as 3° are available. There is also the possibility that tilt angles only slightly larger than the relief angle might allow the point of flow control to move from the top surface of the screen down into the slot opening, which would invalidate the model presented here. Screens with tilt angles approximately equal to or less than the relief angle were not tested in this study, so the exact upper limit on the tilt angle relative to the relief angle is unknown.

Screen Inclination, Drop Height, and Arc Radius

Changes in screen inclination, drop height to the start of the screen, and total drop height across the structure affect capacity primarily by increasing the specific energy in (9), and secondarily by changing the Froude, Reynolds, and Weber numbers, and thus the values of C_F and C_{cv}. Steeper screens exclude finer debris and smaller fish, but at the expense of more head drop for a given length of screen.

Concave screen panels have increased capacity due to the increased pressure on the screen face, and allow a longer length of screen for a given structural height and head drop. Use of a concave screen also flattens the discharge trajectory of the overflow jet whose energy must be dissipated downstream from the screen.

CONCLUSIONS

A theoretically based model for hydraulic performance of Coanda-effect screens has been presented, and a computer program to implement the model has been developed. The model predicts the depth and velocity profiles across a Coanda-effect screen using the equation for spatially varied flow with decreasing discharge. The flow over the screen surface is unaffected by hydraulic friction. In addition to the flow profile, the model predicts the total flow through the screen surface, the overflow off the toe of the screen, and the wetted length of screen when there is no overflow. The model includes a relation developed in this study to predict the flow through tilted-wire screening surfaces. The relation uses a modified orifice equation that incorporates the effects of the Froude number of the flow over the screen and the Reynolds and Weber numbers of the flow past the screen slot.

The model was used to predict the performance of several prototype-size Coanda-effect screen structures. Predicted and observed flow rates and wetted screen lengths compared favorably for nearly 100 tests spanning a range of hydraulic conditions. The model provides designers with a tool that can be used to accurately estimate screen capacity and develop economical screen structures for a variety of objectives and site conditions.

ACKNOWLEDGMENTS

The writer wishes to thank Robert Einhellig and Warren Frizell for their many valuable suggestions incorporated into the laboratory studies and the model presented here. Experimental data collection and model development were funded by the U.S. Bureau of Reclamation's Science and Technology Program (projects ER.99.29, ER.99.10, and NM022). Additional experimental data were collected in connection with a cooperative agreement with the Metro Wastewater Reclamation District, Denver. James Strong, Robert Weir, and John Brandt provided sample screens for testing, and Robert Weir suggested the optical reflection method used to measure wire tilt angles. The optical comparator measurements of wire tilt angles were made by Eric Stanfield and Shira Fishman of the National Institute of Standards and Technology, Gaithersburg, Md.

REFERENCES

Babb, A. F., and Schlenker, S. (1999). ''Flow through perforated floor plates on supercritical slopes.'' *Proc., 1999 Water Resour. Engrg. Conf.*, ASCE, Reston, Va.

Chow, V. T. (1959). *Open-channel hydraulics*, McGraw-Hill, New York, 327–333.

Fontein, F. J. (1965). ''Some variables influencing sieve-bend performance.'' *Proc., Int. Chemical Engrs. Joint Meeting*, New York.

Miao, L.-S. (1958). ''An investigation of flow through an open channel with screen bed.'' *The Trend in Engineering*, October, 14–17.

Nasser, M. S., Venkataraman, P., and Ramamurthy, A. S. (1980). ''Flow in a channel with a slot in the bed.'' *J. Hydr. Res.*, Delft, The Netherlands, 18(4), 359–367.

Noseda, G. (1955). ''Operation and design of bottom intake racks.'' *Proc., 6th General Meeting*, IAHR, Delft, The Netherlands, C17-1 to C17-11.

Ramamurthy, A. S., Zhu, W., and Carballada, B. L. (1994). ''Flow past a two-dimensional lateral slot.'' *J. Envir. Engrg.*, ASCE, 120(6), 1632–1638.
Strong, J. J., and Ott, R. F. (1988). ''Intake screens for small hydro plants.'' *Hydro Review*, VII(V), 66–69.
Venkataraman, P. (1977). ''Divided flow in channels with bottom openings.'' *J. Hydr. Div.*, ASCE, 103(2), 1900–1904.
Wahl, T. L. (1995). ''Hydraulic testing of static self-cleaning inclined screens.'' *Proc., 1st Int. Conf. on Water Resour. Engrg.*, ASCE, New York, 1224–1228.
Wahl, T. L. (2000). ''Hydraulic tests of proposed Coanda-effect screens for Fulton Ditch: Phase I test results.'' *Memo. Rep. PAP-857*, Water Resour. Res. Lab., U.S. Bureau of Reclamation, Denver.

NOTATION

The following symbols are used in this paper:

C_{cv} = combined contraction and velocity coefficient;
C_F = coefficient related to alignment of approach flow with screen opening; a function of Froude number;
D = flow depth;
E = specific energy;
F = Froude number;
g = acceleration of gravity;
H_a = drop height from crest of acceleration plate to top of screen;
H_s = head drop from upstream pool to top of screen;
n = Manning roughness coefficient;
p = screen porosity, $s/(s + w)$;
q = unit discharge;
q_{bypass} = unit discharge off toe of screen;
q_{inflow} = unit discharge at top of screen;
q_{screen} = unit discharge through screen surface;
R = Reynolds number;
r = screen arc radius;
S_f = friction slope;
s = open slot width between wires;
s' = length of slot opening from trailing edge of one wire to leading edge of next downstream wire, $\sqrt{s^2 + y_{off}^2}$;
V = velocity tangent to screen surface;
$\mathbf{V}_r$ = magnitude of resultant velocity vector approaching screen slot opening;
W = Weber number;
w = screen wire width;
y_{off} = offset height created by tilted wire;
α = energy coefficient;
ψ = angle between screen surface and line connecting leading edge of one wire to trailing edge of upstream wire;
Δq = unit discharge through screen slot;
δ = deflection angle of velocity vector approaching screen slot opening;
ε = deflection angle from tail of one wire to leading edge of next downstream wire, relative to top surface of wire;
ϕ = wire tilt angle;
λ = wire relief angle;
ν = kinematic viscosity;
ρ = fluid density;
σ = surface tension force per unit length;
θ = angle of screen surface, measured from horizontal;
θ_s = included angle of screen arc; and
θ_0 = incline angle of screen from horizontal at top of screen.

Subscripts

1 = upstream end of control volume; and
2 = downstream end of control volume.